LARGE EDDY SIMULATION OF OPEN-CHANNEL FLOW OVER AND THROUGH TWO LAYERS OF SPHERES

Thorsten Stoesser[1] , Jochen Fröhlich[2], Wolfgang Rodi[3]

ABSTRACT

The paper investigates the role of porosity of a permeable wall and the interaction between the interstitial and the outer flow. This situation is, among others, relevant for sediment transport and bed friction in natural channels. The study employs detailed large eddy simulations of a prototype situation, where the wall consists of two layers of spheres with the same diameter and their centers being arranged on a cubic lattice. The domain covers a total of 432 spheres. The recorded time- and space-resolved data are averaged and compared to recent measurements at the University of Aberdeen finding good agreement. The high porosity of the bed induces considerable momentum exchange between the outer flow and within the spheres. This generates additional shear stresses and hence leads to velocity and turbulence intensity distributions differing considerably from those over solid beds. Coherent flow structures, like sweeps and ejections are shown to occur and are suggested to be the driving mechanism of momentum exchange. Below the roughness interface, flow velocities, turbulence intensities and pressure fluctuations are damped exponentially which is also in line with experimental data.

1. INTRODUCTION

Although almost all natural channels have permeable beds such as gravel-bed rivers, very little research has been undertaken in order to study the effect of channel bed permeability on the mean and instantaneous flow. In common practice a permeable bed has usually been treated analogously to an impermeable bed and flow resistance coefficients and velocity distributions were derived irrespective of bed porosity. However, depending on the permeability of the subsurface there are significant interaction processes between the flow above the porous bed and the subsurface area.

[1] Research Associate, Institute for Hydromechanics, Karlsruhe University, 76128 Karlsruhe, Germany (stoesser@ifh.uka.de)

[2] Research Associate, Institute for Technical Chemistry and Polymer Chemistry, University of Karlsruhe, 76128 Karlsruhe, Germany (froehlich@ict.uni-karlsruhe.de)

[3] Professor, Institute for Hydromechanics, Karlsruhe University, 76128 Karlsruhe, Germany (rodi@ifh.uka.de)

The effects of interaction are a non-zero (slip) velocity at the permeable boundary (see Figure 1) and the existence of turbulent exchange of mass and momentum between the two flow regions. These exchange processes are responsible for additional shear stresses near the boundary (Nezu, 1977). For instance, Lovera and Kennedy (1969), Zagni and Smith (1976), and Zippe and Graf (1983) have shown that the overall friction loss in a flow over a permeable bed is larger than over an equivalent impermeable bed. The driving force that is responsible for the exchange processes between the pore layer and the upper flow is the presence of local pressure gradients, a mechanism similar to the interaction between the turbulent boundary layer and the viscous sublayer in the flow over a smooth bed (see Figure 1, taken from Nezu, 1977). These local pressure gradients are generated by the dynamics of the turbulent flow over (smooth, rough, and permeable) boundaries, where the flow field is dominated by energetic three-dimensional organized (coherent), vortical structures. Over 4 decades of experimental work have been dedicated to the identification of the physical processes which govern these coherent structures, and much progress has been made in recent years due to the advances in measurement methods and in numerical simulation techniques associated with the growth in speed and capacity of modern supercomputers. Whereas the flow physics of coherent structures over smooth surfaces is understood fairly well (see the summary by Robinson, 1991), the flow over rough impermeable and permeable walls is still an area of active turbulence research. The reason is that there exists a wide variety of possible wall roughness geometries as well as permeability conditions and recent research endeavors have shown that the details of the geometry influence the flow across the entire turbulent layer (Jiménez, 2004). As a consequence, the distribution of mean flow velocities and higher order turbulent statistics differ considerably from those over smooth walls in a region usually called the "roughness sublayer", which is a layer adjacent to the rough (im)permeable bed. There have been numerous research efforts recently to quantify the effects of (impermeable) roughness on the mean flow statistics (see the most recent summary by Jimenez, 2004) or to elucidate the turbulent instantaneous flow structures (Stoesser et al., 2003) over impermeable rough beds. Studies of turbulent flow over permeable beds are very scarce. There has been few experimental work on quantification of the friction loss (Kong and Schetz, 1982, Zagni and Smith, 1976, Zippe and Graf 1983), on the determination of the vertical velocity profile for the flow above the permeable bed (Gupta and Paudyal, 1986, Zagni and Smith, 1976, Zippe and Graf 1983, Nakagawa et al., 1991, Dancey et al., 2000) as well as on the collection of pressure and velocity signals within the permeable bed (Detert et al., 2004). There are several numerical studies of flow over and/or through porous media which use an integral numerical approach like the Volume Average Navier Stokes (VANS) approach (Breugem and Boersma, 2005) or apply adequate slip-conditions (Jiménez et al., 2001), but these methods do not resolve the details of the interaction between the two layers, hence important physical mechanisms may be neglected. Directly resolving the details of the flow geometry of a porous media is extremely complex and tremendously expensive especially for natural permeable beds. To our knowledge there is only one study that represents the porous media directly (Breugem and Boersma, 2005). Breugem and Boersma (2005) performed a DNS over and through a permeable bed that consisted of an array of cubes, with the main objective of validating a previously developed integral approach.

In this paper we present the results of a LES of open-channel flow over a permeable bed that consists of two layers of spheres. This is the first detailed numerical study of the flow over a permeable bed that has also been investigated in a laboratory experiment. A related simulation with three layers of spheres will be presented shortly (Stoesser et al. 2007). The main purpose of the present study is to provide further insight into the turbulent flow over permeable beds and to enhance the understanding of the effect of bed permeability on the mean and instantaneous flow. Temporal and spatial averaging is used to quantify the effects on the flow velocities and the three components of turbulence intensities. We furthermore show the existence of coherent flow structures and their effect on the mass and momentum exchange processes between the flow above the bed and the subsurface region.

2. NUMERICAL FRAMEWORK

The LES code MGLET, originally developed at the Institute for Fluid Mechanics at the Technical University of Munich (Tremblay and Friedrich, 2001), was used to perform the Large Eddy Simulations. The code solves the filtered Navier-Stokes equations discretised with a finite-volume method on a staggered Cartesian grid. Convective and diffusive fluxes are approximated with central differences of second order accuracy and time advancement is achieved by a second order, explicit Adams-Bashford scheme. A Poisson equation is solved to couple the pressure to the velocity field. The subgrid-scale stresses appearing in the filtered Navier-Stokes equations are computed using the dynamic approach of Germano *et al.* (1991). The no-slip boundary condition is applied on the surface of the spheres where the immersed boundary method is employed (Verzicco *et al.*, 2000). This method is a combination of applying body forces in order to block the cells that are fully inside the sphere and a Lagrangian interpolation scheme of third order, which is used for the cells that are intersected by the spheres' surface to maintain the no-slip condition (Tremblay and Friedrich, 2001).

3. SETUP AND BOUNDARY CONDITIONS

The setup and boundary conditions of the Large Eddy Simulation are selected in analogy to flume experiments performed by Pokrajac (2005) at the University of Aberdeen, where spheres of $D=12mm$ diameter were placed in two layers on the flat bottom. The flow depth from the roughness tops to the free surface is $H=41\ mm$ which gives a relative submergence ratio of $H/D=3.42$. The depth-averaged bulk velocity is $U=0.43\ m/s$, which yields a Reynolds number of $Re= UH/\nu \approx 17600$. Mean flow velocities were measured with a two-dimensional Particle Image Velocimetry (PIV) system along two longitudinal (x-z) planes above the spheres. These measurements are used in order to validate the results of the LES computations. The computational domain of the surface flow region spans $5.3H$ x $3.5H$ x H. The subsurface region consists of two layers of spheres of diameter $D=12\ mm$ arranged in a cubic pattern with 18 x 12 spheres per layer (Figure 2). In the top left part of Figure 2a sketch with a part of the setup is given indicating planes with maximum (plane 1) and minimum porosity (plane 2). A very high resolution grid consisting of $720 \times 480 \times 172$ points for the computation domain is employed, which is approximately 60 million grid points in total. Hence, each sphere is resolved with 40 points over the diameter. Based on the global wall shear stress, the grid spacings in terms of wall units are $\Delta x^+ \approx 8$ in streamwise direction and $\Delta y^+ \approx 8$ in spanwise direction. In the vertical direction the grid spacing is kept at a constant value of $\Delta z^+ \approx 1.0$ from the bed to the top of the spheres and is stretched above the spheres towards the surface. A longitudinal and a plane view of the grid, where only every 5th grid line is plotted is given in Figure 3. In the top left part of Figure 3 a sketch with a part of the domain is given indicating four points where time-signals are recorded. It has to be noted that due to the third order interpolation scheme of the immersed boundary method the touching point is not a singular point but an area consisting of 3 x 3 grid points. This is the reason why later on in plots with maximum porosity a trace of the sphere is still visible. Periodic boundary conditions are applied in the streamwise and spanwise directions in order to simulate an endless channel with fully developed flow conditions.

4. RESULTS AND DISCUSSION

4.1 Mean Flow

Figure 4 shows contours of the time-averaged streamwise velocity along a longitudinal plane with minimum porosity (indicated as plane 1 in the top left part of Figure 3) for both experiment (left) and LES. Overall, the match between simulation and experiment is very good and

differences can only be observed near the top of the spheres, where the LES predicts a slight acceleration of the flow. Between the roughness elements near the sphere tops small recirculation regions can be seen, which are caused by separation at the top of the spheres. This small-scale behavior could not be measured in the laboratory due to the resolution of the camera. Figure 5 compares the mean-flow velocities between LES and experiments in a longitudinal plane with maximum porosity i.e. where the spheres touch each other (indicated as plane 2 in the top left part of Figure 3). Again the agreement between measured and calculated flow velocities is very good. Due to the relatively large porosity of the setup there is non-zero flow in the pore region. In the measurements the plane between spheres cannot be measured due to the spheres obstructing the camera view.

Figure 6 shows a more quantitative comparison of mean streamwise flow velocities along several vertical lines along two longitudinal planes with minimum porosity (left) and maximum porosity (right). As was shown before, the prediction of the mean streamwise velocity is in an excellent agreement with the observed data and there are only small differences. The spatial variation of streamwise velocity profiles along the two planes can hardly be discerned; this suggests the existence of only a thin roughness layer, i.e. the layer where the flow "feels" the details of the roughness geometry. However, the acceleration of the flow on the top of the spheres, recirculation behind the spheres and a certain amount of flow through the pores can be seen clearly. The flow velocities in the first pore are slightly smaller than in the second pore near the flume bed. This has also been reported by Prokrajac (2005) and now confirmed with the present LES. The reason for this behavior is that the turbulent exchange process between the outer flow region and pore region causes a retardation of the streamwise flow in the first layer or in the first pores respectively.

The protrusion of turbulence into the pores can be quantified with streamwise, spanwise and wall normal turbulence intensities. Figure 7 shows the three spatially-averaged components normalized with the global shear velocity $\langle u' u' \rangle^{1/2}/u_\tau$, $\langle v' v' \rangle^{1/2}/u_\tau$, $\langle w' w' \rangle^{1/2}/u_\tau$. It is interesting to see that the peaks of all components are located at the top of the permeable bed, i.e. at *z/H=0*. Unfortunately, for this setup Prokrajac (2005) did not evaluate turbulence intensities and hence a comparison is made with experimental data obtained by Grass (1972). Though Grass measured flow and turbulence above one layer of uniform gravel (with *k=9mm* and a relative submergence ratio of *H/D=5.5)* the normalized profiles are very similar. Grass (1972) also observed large peaks in the streamwise component near the bed as well as in the shear stress (Figure 7, right). It can be seen that considerable turbulence intrudes into the subsurface area and the effect of mass and momentum exchange becomes obvious from the fairly high values of wall-normal fluctuations in the first layer of spheres (*z/H=0* to *z/H=0.3*), which are of similar magnitude as the streamwise fluctuations. Further below, i.e. in the second layer of spheres, there is still considerable turbulence left, however the wall-normal component is not so strong anymore.

4.1 Instantaneous Flow

Figure 8 shows contours of instantaneous wall-normal velocities in longitudinal planes with minimum porosity (upper part) and maximum porosity (lower part). The colors (blue indicates strong downward movement $w < 0$ and red indicates strong upward movement of fluid with $w > 0$) illustrate the existence of coherent structures which prevail over the entire channel depth. Near the bed the sweeps and ejections seem to occur more often. On the other hand, as was shown in a previous paper (Stoesser et al., 2005), vortices grow as they travel towards the free surface.

Figure 9 presents snapshots of the perturbation vector field (*u'-w'*) in two selected *x-z* planes with minimum (left) and maximum (right) porosity, respectively. It is apparent from the magnitude of the perturbation vectors that most of the turbulence occurs in the roughness sublayer just above the spheres. In the slice with maximum porosity, in- and outflow scenarios are visible (e.g. at

x/D=7.8 and *x/D = 5.5*). In the plane with minimum porosity an ejection event (i.e. *u'<0* and *w'>0*, at *x/D=3.5, y/D=0.5*) can be observed and a sweep event (i.e. *u'>0* and *w'<0*) can be spotted in the plane with maximum porosity at *x/D=6.5, y/D=0.5*. These events are comparable to those observed over smooth beds (as described in Robinson, 1991) and rough beds (Stoesser et al. 2003).

The instantaneous data were also analyzed using a quadrant analysis, similar to Raupach (1981). The instantaneous values of *u'* and *w'* are classified into four quadrants *i* which are defined as outward interaction (*i=1*, where *u'>0* and *w'>0*), ejections (*i=2*, where *u'<0* and *w'>0*), inward interaction (*i=3*, where *u'<0* and *w'<0*) , and sweeps (*i=1*, where *u'>0* and *w'<0*), respectively. At any point in the flow, the contribution of events of different strength to the total Reynolds stress from quadrant *i* can be computed by the formula (Raupach, 1981):

$$\langle u'w' \rangle_{i,L} = \lim \int_0^T u'(t)\, w'(t)\; I_{i,L}(u'w')\; dt$$

$$I_{i,L}(u'w') = \begin{cases} 1 & \text{if } (u',w') \text{ is in quadrant } i \text{ and if } |u'w'| \geq L|<u'w'>|, \\ 0 & \text{otherwise} \end{cases}$$

Figure 10 does not show the conditional mean $\langle u'w' \rangle_{i,L}$ but the probability $P_{i,L} = \lim \int_0^T I_{i,L}(u'w')\; dt$ of events with strength *L=0, 1, 2,… , 19*. Note that by definition $\sum_i P_{i,L=0} = 1$. This quantity is shown for the four selected locations in Figure 3 at which time-signals were collected over a period of *10* flow-through times. The dominance of sweeps and ejections is immediately apparent at the locations 3 and 4, which is *0.5D* above the bed, a fact that has also been seen above rough impermeable beds (Stoesser et al., 2003). This dominance can as well be observed at location 2, which is in the centre of the first pore. This is clear evidence that sweeps and ejections are mainly responsible for mass and momentum exchange processes. It is also evident that these processes occur during strong events, which is apparent from the relatively flat probability curve showing that about one third of the events are 19 times larger than the average Reynolds stress. The amount of strong events seems less pronounced at location 3, which is *0.5D* above the center of the pore. However, at that location the mean value of $<u'w'>$ is very high so that the number of extreme events decreases. Near the bottom wall at location 1 there seems to be no dominating event anymore and the probability distribution takes a hyperbolic shape, which indicates isotropic turbulence.

4. CONCLUSIONS

Results were presented of a large eddy simulation of open channel flow over a permeable bed consisting of two layers of spheres. In these simulations the unsteady flow around and between the individual spheres was resolved to a very high degree which provides an enormous wealth of data. The calculated mean velocities showed generally good agreement with the measured data of Prokrajac (2005). First findings concerning higher order statistics and flow structures were reported. These are currently extended in ongoing work.

ACKNOWLEDGEMENTS

This work is part of a research project funded by the German Research Foundation (DFG) under project number Ji 18/10-3. The computations were carried out on the IBM SP-SMP of the scientific supercomputing centre (SSCK) at the University of Karlsruhe. The provision of the experimental data by Dr. Dubravka Prokrajac and the successful collaboration with the Department of Engineering at the University of Aberdeen is acknowledged gratefully.

REFERENCES

Breugem, W.P., Boersma, B.J. (2005). Direct Numerical Simulations of Turbulent Flow Over a Permeable Wall Using a Direct and a Continuum Approach. *Physics of Fluids*, 17(2).

Dancey, C.L., Balakrishnan, M., Diplas, P., Papanicolaou, A.N. (2000). The Spatial Inhomogeneity of Turbulence Above a Fully Rough, Packed Bed in Open Channel Flow", *Experiments in Fluids*, 29, pp. 402-410.

Detert, M., Jirka, G.H., Jehle, M., Klar, M,. Jähne, B., Köhler, H.-J., Wenka, T. (2004). Pressure Fluctuations Within Subsurface Gravel Bed Caused by Turbulent Open-Channel Flow, *Proc. River Flow 2004*, M. Greco (Ed.), Napoli, Italy.

Germano M., Piomelli U., Moin P., Cabot W. H. (1991). A Dynamic Subgrid-scale Eddy Viscosity Model. *Physics of Fluids*, 3(7), 1760-1765.

Gupta, A. D., Paudyal, G. N. (1985) Characteristics of Free Surface Flow over a Gravel Bed. Journal of Irrigation and Drainage Engineering. Vol. 111, no. 4, pp. 299-318.

Grass, A. J. (1972). Structural Features of Turbulent Flow Over Smooth and Rough Boundaries. *J. of Fluid Mechanics*, Vol. 50 No. 2, pp 233-255.

Jiménez, J. (2004). Turbulent Flows Over Rough Walls. *Annu. Rev. Fluid Mech.*, 36, 173–96.

Jiménez, J., Uhlmann, M., Pinelli, A., Kawahara, G. (2001). Turbulent Shear Flow over Active and Passive Porous Surfaces. *J. of Fluid Mechanics*, Vol. 442 No. 9, pp 89-117.

Kong, F. Y., Schetz, J. A. (1982). Turbulent Boundary Layer over Porous Surfaces with Different Geometries. *AIAA Paper* 82-0030.

Lovera, F., Kennedy, J. F. (1969). Friction-Factors for Flat-Bed Flows in Sand Channels *ASCE J Hydraul Div*, Vol. 95, No 4, pp 1227-1234.

Nakagawa, H., Tsujimoto, T., Shimizu, Y. (1991). Turbulent Flow with Small Relative Submergence. *Fluvial Hydraulics of Mountain Regions*. Editor: A. Armanini, G. Di Silvio, Lecture Notes in Earth Sciences, Vol. 37, pp.33-44

Nezu, I. (1977). "Turbulent Structure in Open-Channel Flows." Ph.D Thesis, Dept. of Civil Engineering, Kyoto Univ., Japan.

Prokrajac (2005). Personal Communication

Raupach, M. (1981). Conditional Statistics of Reynolds Stress in Rough-Wall and Smooth-Wall Turbulent Boundary Layers. *J. of Fluid Mechanics*, Vol. 108 pp 363-382.

Robinson, K. (1991). Coherent Motions in the Turbulent Boundary Layer, *Ann. Rev. Fluid Mech*. Vol. 23. pp 601-639.

Stoesser, T., Fröhlich, J., Rodi W. (2003). Identification of Coherent Flow Structures in Open Channel Flow over Rough Bed Using Large Eddy Simulation. *Proceedings 30th IAHR Congress*, Thessaloniki, Greece.

Stoesser, T., Rodi, W., Fröhlich, J. (2005). Large Eddy Simulation of Open-Channel Flow Over a Layer of Spheres. In: *Proc. of 31st IAHR Congress*, Seoul, Sep. 11-16.

Stoesser, T., Fröhlich, J., Rodi, W. (2007). Turbulent Open-Channel Flow over a Permeable Bed, submitted *to 32th IAHR Congress*, Venice, 2007.

Stone, H.L. (1968). Iterative Solution of Implicit Approximation of Multi-dimensional Partial Differential Equations. *SIAM J. Numerical Analysis*. No. 3.

Tremblay, F., Friedrich, R. (2001). An Algorithm to Treat Flows Bounded by Arbitrarily Shaped Surfaces with Cartesian Meshes. In: *Notes on Numerical Fluid Mechanics*, Vol. 77, Springer.

Verzicco, R., Mohd-Yusof, J., Orlandi, P., Haworth, D. (2000). Large Eddy Simulation in Complex Geometric Configurations Using Boundary Body Forces. *AIAA J.* 38 (3). pp 427ff.

Zagni, A. F. E., Smith, K. V. H. (1976). Channel Flow over Permeable Beds of Graded Spheres. *ASCE, J. of the Hydraulics Division*, Vol. 102, No. 2. pp 207-222.

Zippe, H. J, Graf, W. H. (1983). Turbulent Boundary-Layer Flow over Permeable And Non-Permeable Rough Surfaces. *J. of Hydraulic Research* Vol. 21, No. 1, pp 51-65.

FIGURES

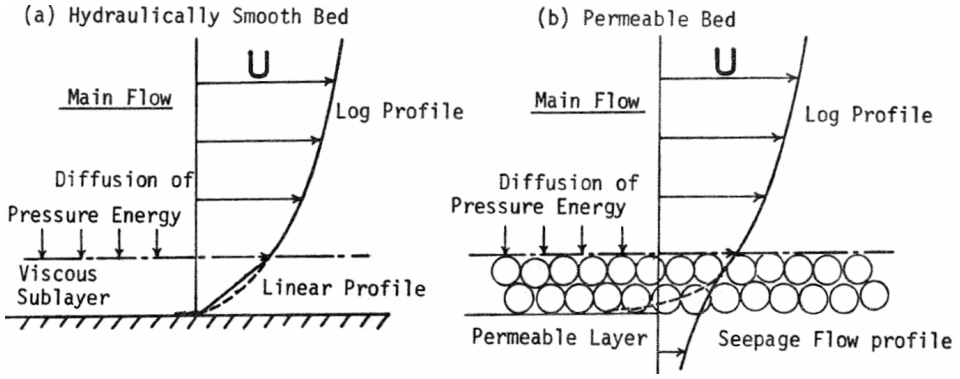

Figure 1: Analogy between smooth bed flows and flows over a rough permeable bed (Nezu, 1977).

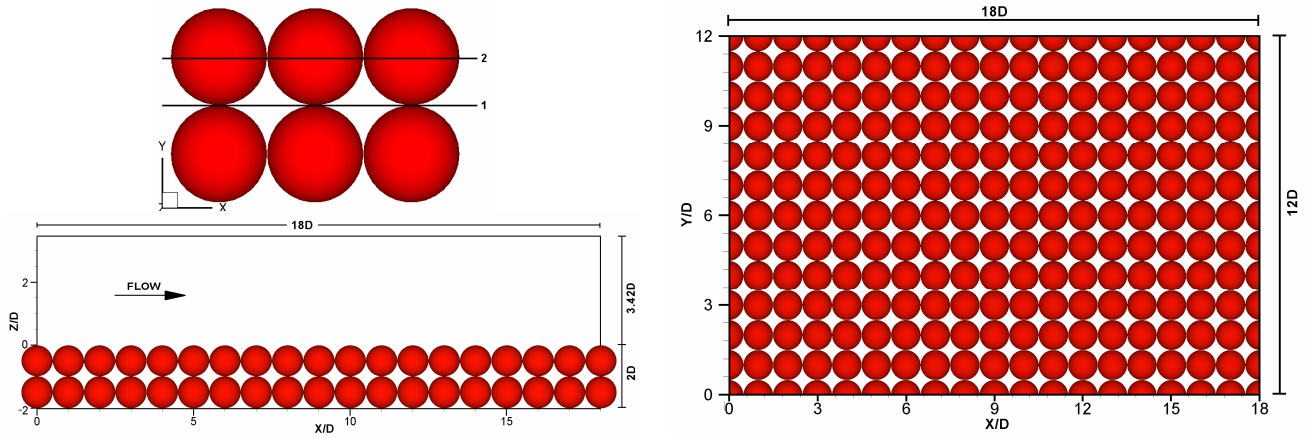

Figure 2: Setup of the Large-Eddy Simulation in longitudinal (bottom left) and plane view (right) as well as a sketch (top left) indicating planes of maximum (Plane 1) and minimum (Plane 2) porosity.

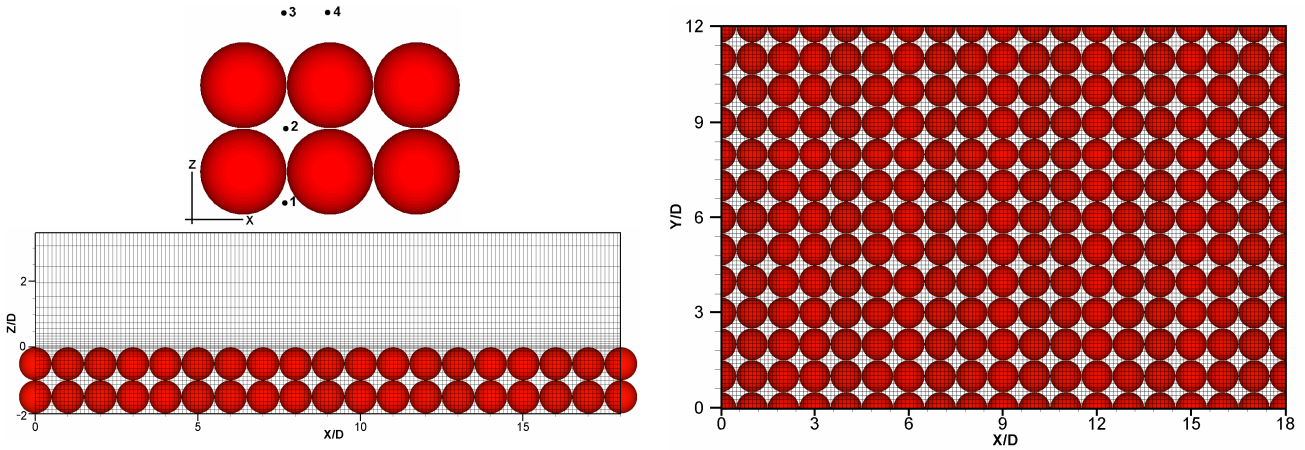

Figure 3: Grid (only every 5th grid line is shown) of the Large-Eddy Simulation in longitudinal (bottom left) and plane view (right) as well as a sketch (top left) indicating points (1-4) where time-signals were recorded.

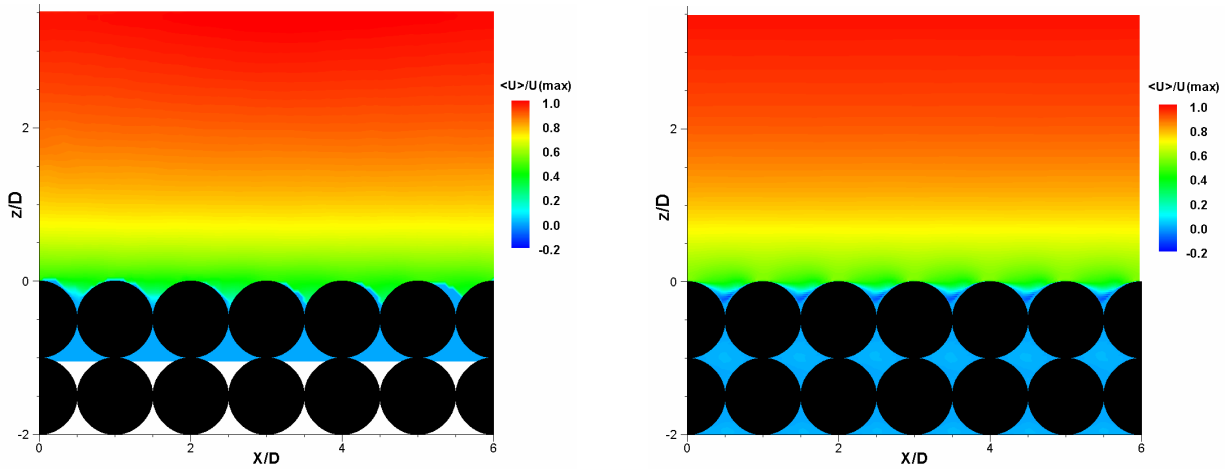

Figure 4: Contours of time-averaged streamwise velocity <*u*> in a plane with minimum porosity as measured in the laboratory (left) and predicted with LES (right)

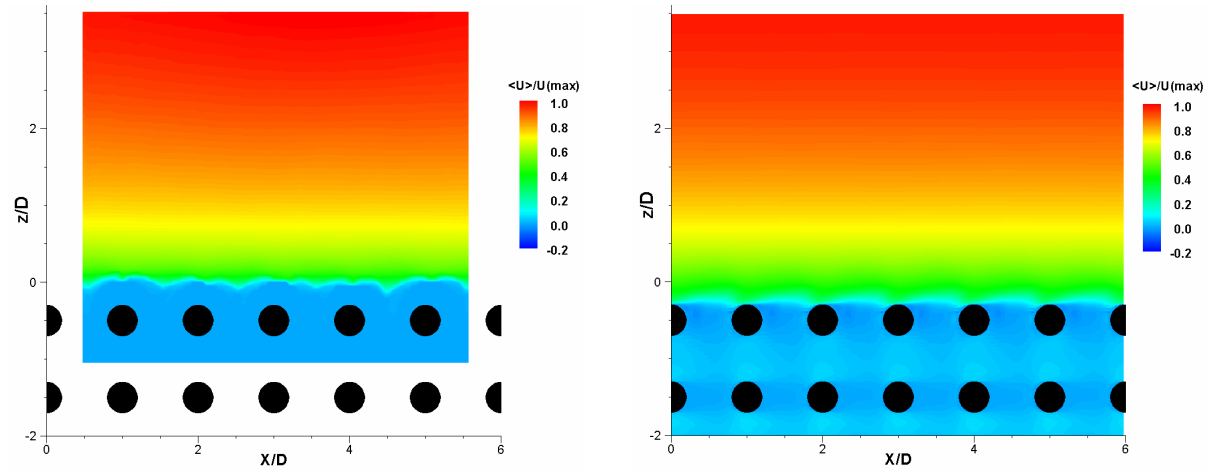

Figure 5: Contours of time-averaged streamwise velocity <*u*> in a plane with maximum porosity as measured in the laboratory (left) and predicted with LES (right)

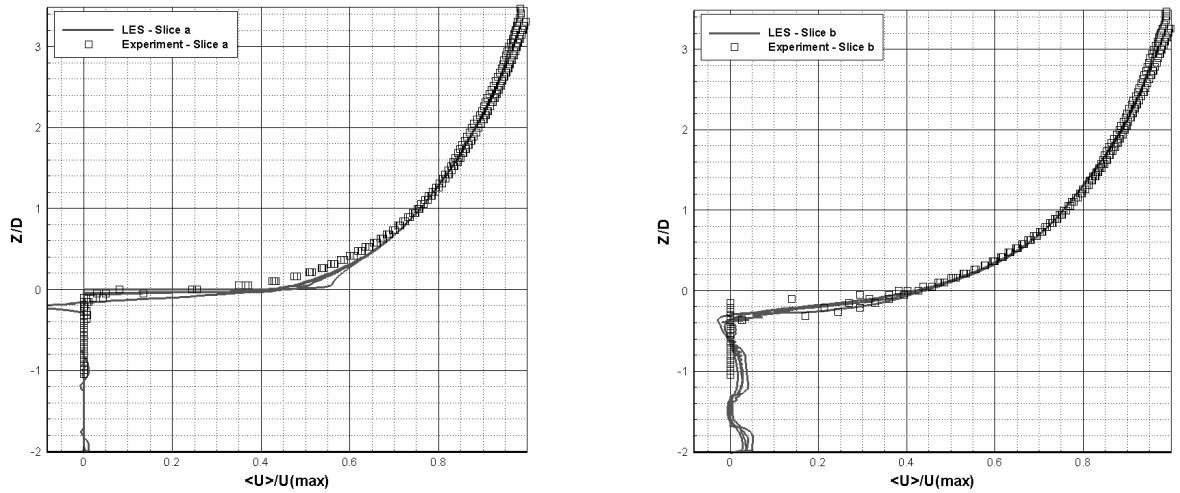

Figure 6: Quantitative comparison of mean streamwise velocity between experiments (squares) and LES (solid lines) along several verticals in planes with minimum (left) and maximum (right) porosity

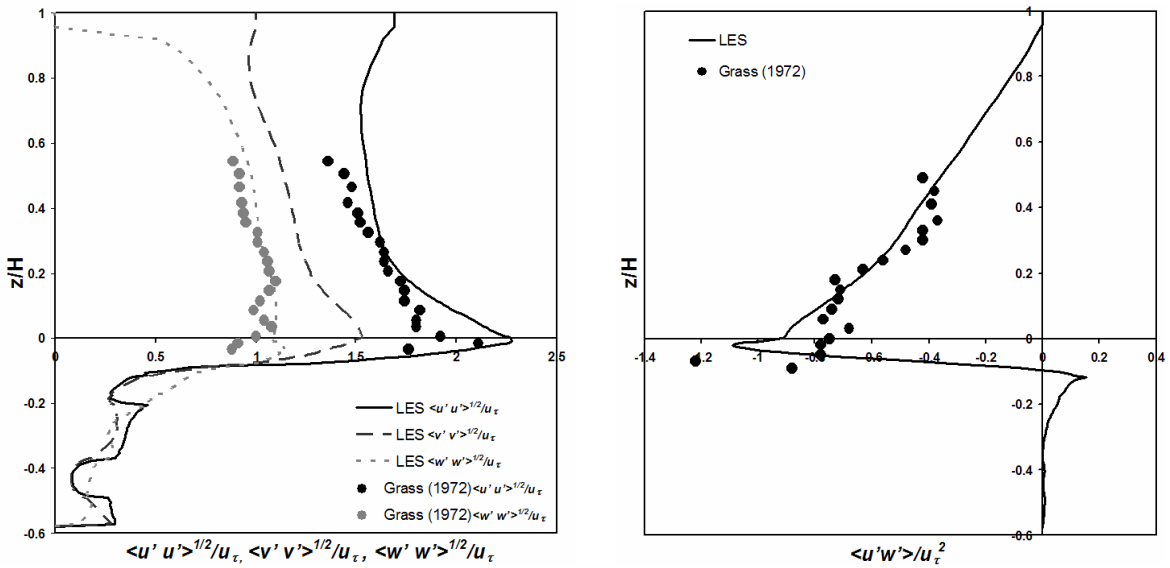

Figure 7: Spatially averaged vertical distribution of normalized turbulence intensities ($\langle u' u' \rangle^{1/2}/u_\tau$, $\langle v' v' \rangle^{1/2}/u_\tau$, $\langle w' w' \rangle^{1/2}/u_\tau$, right) and the normalized shear stress ($\langle u'w' \rangle/u_\tau^2$, left)

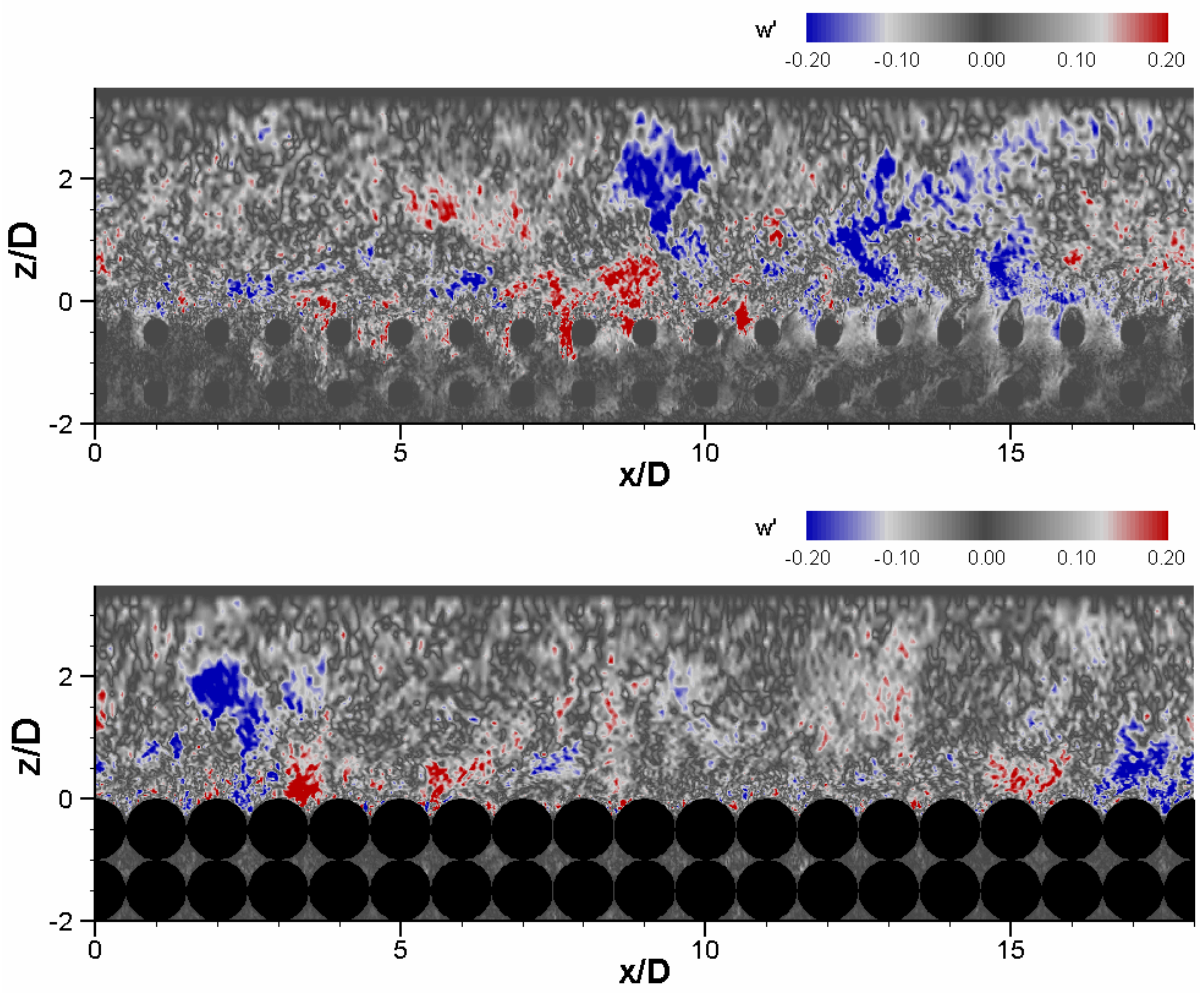

Figure 8: Instantaneous wall-normal turbulent fluctuations $w'=w-\langle w \rangle$ in two selected longitudinal planes with maximum (upper) and minimum (lower) porosity.

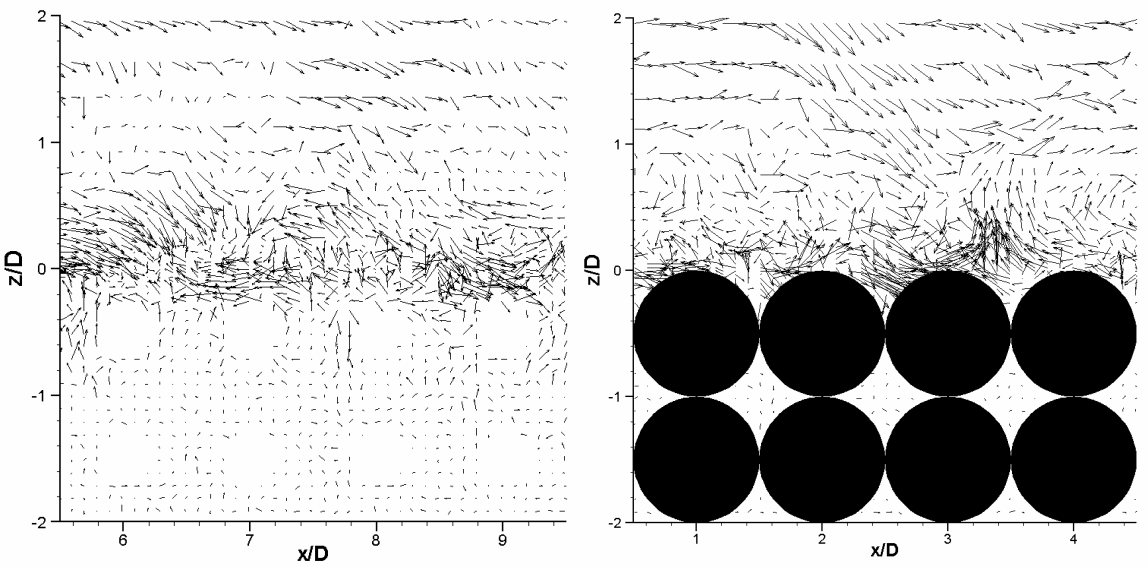

Figure 9: Snapshots of perturbation vectors (*u'-w'*) in *x-z* planes with minimum (left) and maximum (right) porosity from LES.

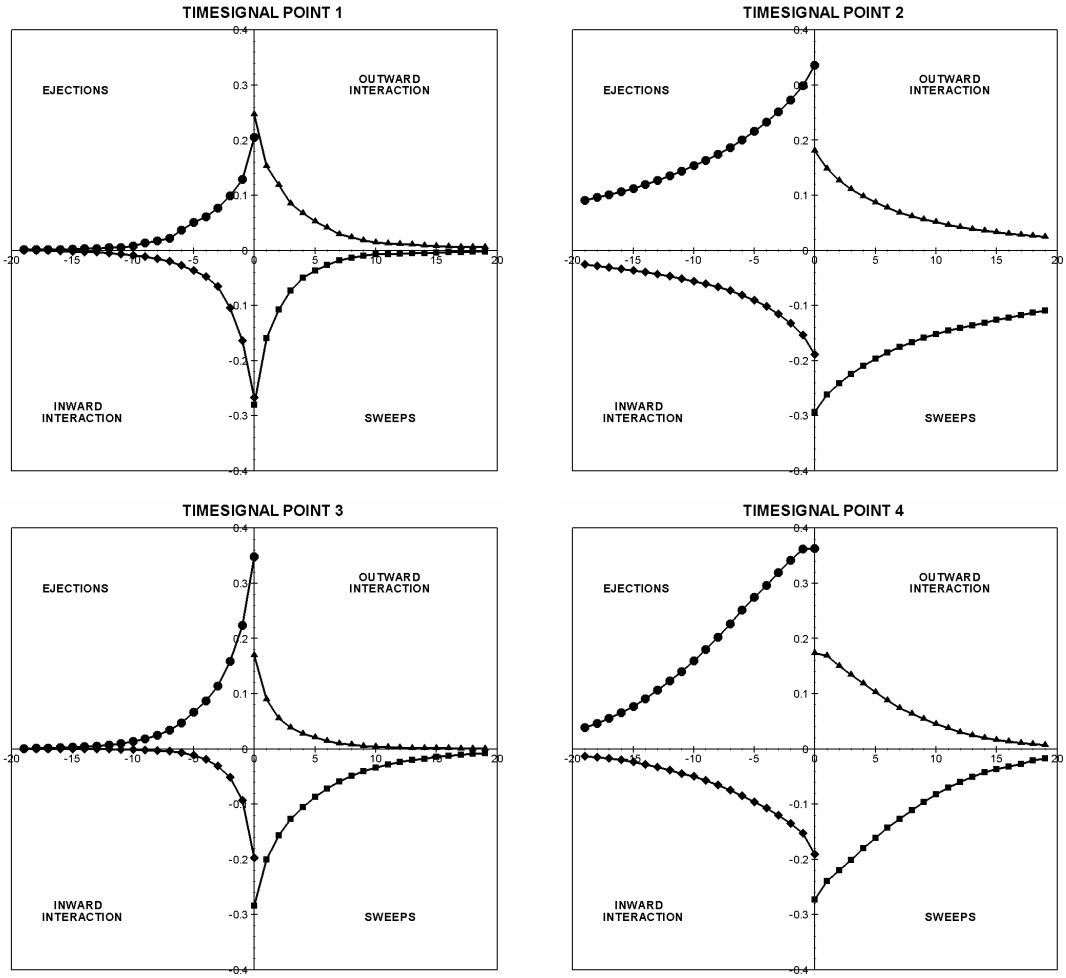

Figure 10: Probability of quadrant events at the four points in the flow field specified in Figure 3. The horizontal axis is, for each quadrant, *sign(u')L* and the vertical axis *sign(w') $P_{i,L}$* . Each symbol represents an evaluation with a particular value of *L=0,1,2, ... 19*.